Insights into the Dynamics and Binding Mechanisms of the Alkhumra Virus NS2B/NS3 Protease: A Molecular Dynamics Study

Jurica Novak,* Shivananda Kandagalla, and Ramesh Sistla

Alkhumra virus, a zoonotic pathogen in the Flaviviridae family, causes severe hemorrhagic fever in humans, yet vaccines and drugs remain unavailable. The nonstructural protein 2B (NS2B)/nonstructural protein 3 (NS3) NS2B/NS3 protease, essential for virion maturation, represents a promising therapeutic target. Structural and dynamical changes induced by NS2B cofactor binding to the NS3 protein are examined using all-atom molecular dynamics simulations. NS2B binding reduces the flexibility of NS3, particularly in contact regions, without altering its secondary structure. Non-bonding van der Waals and electrostatic interactions are identified as the primary driving forces in cofactor binding. The protonation states of catalytic triad residues significantly affect the active pocket's geometry. A drug repurposing campaign utilizing ensemble docking and molecular dynamics simulations identified three DrugBank compounds as potential NS2B/NS3 protease inhibitors. The catalytic serine residue with a deprotonated hydroxyl group contributes most significantly to the free energy of binding. These findings provide a detailed understanding of the molecular interactions underlying ligand binding to NS2B/NS3, offering valuable insights for developing effective inhibitors.

1. Introduction

Alkhumra virus (ALKV), a member of the Flaviviridae family, is an emerging zoonotic pathogen first identified in Saudi Arabia in 1994.[1] Since its discovery, ALKV has been recognized as a significant public health concern in the Middle East, causing sporadic outbreaks of severe hemorrhagic fever with high mortality rates among infected individuals.[2] Despite extensive research efforts,

J. Novak
Centre for Informatics and Computing
Ruđer Bošković Institute
Bijenička cesta 54, Zagreb 10000, Croatia
E-mail: jnovak@irb.hr
S. Kandagalla, R. Sistla
thinkMolecular Technologies
Bengaluru, Karnataka 560102, India

many aspects of ALKV biology, epidemiology, and pathogenesis remain poorly understood.

The virus originally named "Alkhurma" was corrected to "Alkhumra" by the International Committee on Taxonomy of Viruses (ICTV) in 2011 due to a typographical error.[3] However, despite the correction, some authors persist in using the incorrect name "Alkhurma" in their publications. ALKV is primarily transmitted through the bite of infected ticks, primarily *Hyalomma dromedarii*, which serve as the main reservoir host for the virus.[4,5] ALKV is believed to be a zoonotic illness, with potential reservoir hosts such as camels and sheep. Proposed modes of transmission include exposure to an infected vertebrate's blood through a skin wound, being bitten by an infected tick, or consumption of unpasteurized, contaminated milk.[6]

In humans, ALKV infection can lead to a spectrum of clinical manifestations ranging from mild febrile illness to severe hemorrhagic fever and multi-organ failure. The incubation period typically ranges from 3 to 8 days following exposure, after which patients may develop abrupt onset of fever, headache, myalgia, and gastrointestinal symptoms.[7] In severe cases, ALKV infection can progress rapidly to disseminated intravascular coagulation, hepatic dysfunction, and hemorrhagic manifestations, with case fatality rates reported as high as 25%.[8] ALKV is an enveloped, single-stranded RNA virus with a genome of ≈11 kilobases in length. The viral genome encodes three structural proteins (capsid, pre-membrane, and envelope) and seven non-structural proteins involved in viral replication and immune evasion.[9,10] Recent advances in molecular virology have elucidated key aspects of ALKV replication, virulence factors, and host–virus interactions, providing valuable insights into the development of antiviral therapies and vaccines.[11–16]

Currently, the management of ALKV infection primarily relies on supportive care to alleviate symptoms and prevent complications.[17] Patients are provided with supportive therapy, comprising the maintenance of adequate hydration and circulation, ensuring oxygenation and blood pressure levels, and addressing any associated complications.[18] However, these supportive measures do not directly target the underlying viral infection and are associated with limited efficacy in improving patient outcomes. Despite its clinical importance, no specific antiviral

ADVANCED
SCIENCE NEWS

www.advancedsciencenews.com

ADVANCED
THEORY AND
SIMULATIONS

www.advtheorysimul.com

therapies or vaccines are currently available for ALKV infection. The viral nonstructural protein 3 (NS3) protease is a key enzyme involved in viral replication and has emerged as a promising target for the development of novel therapeutic interventions.[19] The NS3 protease plays a crucial role in viral replication by cleaving the viral polyprotein at specific sites, generating functional structural and non-structural proteins required for viral maturation and assembly. This proteolytic processing is essential for maintaining an active infection cycle, making NS3 an attractive antiviral target.[19] Given its similarity to NS3 proteases in other *Flavivirus* (e.g., dengue, Zika, West Nile virus), inhibitors targeting ALKV NS3 could potentially serve as broad-spectrum antivirals against multiple *Flavivirus* infections. Thus, inhibiting NS3 protease activity represents a viable strategy to block viral replication, reduce viral load, and ultimately curtail disease progression in ALKV and related pathogens.

Bessaud et al. identify and purify nonstructural protein 2B (NS2B) and NS3 domains of the ALKV, resulting in a catalytically active viral protease expressed as a hexahistidine recombinant protein.[20] Through in vitro characterization using a *para*-nitroanilide substrate, they provide the first enzymatic properties analysis of this class-4 *Flavivirus* proteinase. This findings underscore the essential role of NS3 association with a short segment of NS2B for protease activity, offering insights for designing inhibitors against ALKV and other pathogenic Flaviviruses. The ALKV NS3 protein exhibits conserved residues at positions His54, Asp75, and Ser138, akin to those observed in the serine protease family.

To the best of our knowledge, there have been no published results regarding the design of ALKV NS3 protease inhibitors. But, the active site of the NS3 protease of Kyasanur forest disease virus (KFDV), the virus most closely related to ALKV, has previously been targeted by small molecules, and a potential allosteric inhibition site was identified.[21,22] In 2022, Kandagalla et al. conducted drug repurposing study targeting KFDV NS3 protease.[21] They identified four FDA approved hepatitis C protease inhibitors as potential inhibitor of KFDV NS3 protease. A molecular dynamics study followed by MM/GBSA binding energy calculation reveals a relatively high free energy of binding, suggesting that the shallow active site may not be suitable for non-covalent inhibitors. In a more recent paper,[22] a new approach was adopted with the main idea to prevent protease activation by allosteric inhibition and disabling the binding of the NS2B cofactor.

In this paper, we explored dynamics of apo NS3 protease and provided evidence how binding of NS2B cofactor influences dynamics by reducing flexibility of NS3 residues. Beside structural insight into NS2B modulation NS3 protease, we performed virtual screening of DrugBank molecules via ensemble docking approach followed by molecular dynamics simulation, finally proposing three compounds as potential inhibitors of NS2B/NS3 complex.

2. Results

2.1. 3D Structure of the ALKV NS2B/NS3 Protease

The amino acid region we focused on for modeling (1381 to 1671 aa) includes the transmembrane part of NS2B, which we re-

moved after creating the model. AlphaFold does not rely on a template for model prediction and refines the model with the Amber-relax option to improve the accuracy of side chain geometry. AlphaFold reports the confidence score of each residue based on the pLDDT (predicted local-distance difference test). The pLDDT score ranges from 1 to 100, with 1 indicating low confidence and 100 indicating high confidence. The model's overall confidence score, displayed in Figure S1 (Supporting Information), was reliable. Ensuring NS2B and NS3 fold correctly is crucial for protease activity. We confirmed this by comparing our NS2B/NS3 protease model with similar proteins from other Flavivirus family.

Being the closest relative to ALKV, we searched for experimentally resolved structures of KFDV NS2B/NS3 protease. Unfortunately, no 3D structure of KFDV NS2B/NS3 protease is available. Given its high sequence similarity (above 50%) with ALKV, the crystal structure of Dengue NS2B/NS3 (PDB ID 3U1I) was chosen for comparison. The comparison, shown in Figure S2 (Supporting Information), clearly demonstrates the correct folding of NS2B and NS3 in our model. Overall, the AlphaFold-generated model seems reliable in terms of protein structure geometry.

2.2. NS2B Cofactor Binding Reduces NS3 Flexibility

To explore the flexibility and conformational dynamics of the NS3 protease, we conducted two sets of molecular dynamics (MD) simulations. Initially, the apo form of the NS3 protein was simulated for 1 (μs), followed by a simulation under identical conditions but with the NS2B cofactor bound. The resulting trajectories were analyzed, and various structural parameters, including root mean square deviation (RMSD), radius of gyration (RoG), root mean square fluctuations (RMSF), and solvent accessible surface area (SASA), were calculated (**Figure 1** and **Table 1**).

The RMSD values for the NS2B/NS3 complex remain relatively stable, averaging 1.97 Å with a standard deviation of 0.26 Å (Figure 1i). In contrast, the free NS3, without the bound NS2B cofactor, exhibits significantly higher flexibility, as indicated by an increase in the average RMSD values to 2.42 Å, with the standard deviation almost twice that of the NS2B/NS3 complex (0.51 Å). The NS2B/NS3 complex, with NS2B binding, encompasses an additional 39 amino acids. This increased volume results in higher RoG values (Figure 1 ii). The standard deviations in both cases are below 1% of the mean RoG values, suggesting a stable globular structure throughout the simulation. The SASA delineates the surface area encompassing a protein, conceptualized with a solvent sphere tangentially touching the molecule's van der Waals contact surface, mirroring the patterns observed in RoG (Figure 1 iii). Figure 1 iv illustrates the flexibility of each residue, quantified by root mean square fluctuation (RMSF). The mean RMSF values demonstrate lower flexibility of amino acid side chains in the NS2B/NS3 complex compared to NS3 alone. Particularly noteworthy is the substantially lower mean RMSF of NS3 (1.25 ± 0.85 Å) within the complex, emphasizing the effect of NS2B. To underscore the structural influence of the NS2B cofactor, the difference in RMSF between free NS3 and the NS2B/NS3 complex (ΔRMSF) is depicted in the lower panel of the figure. ΔRMSF is predominantly positive for most residues, with three regions exhibiting significant positive deviations and one displaying a negative deviation. Regions spanning Val45-Ile50, Glu100-
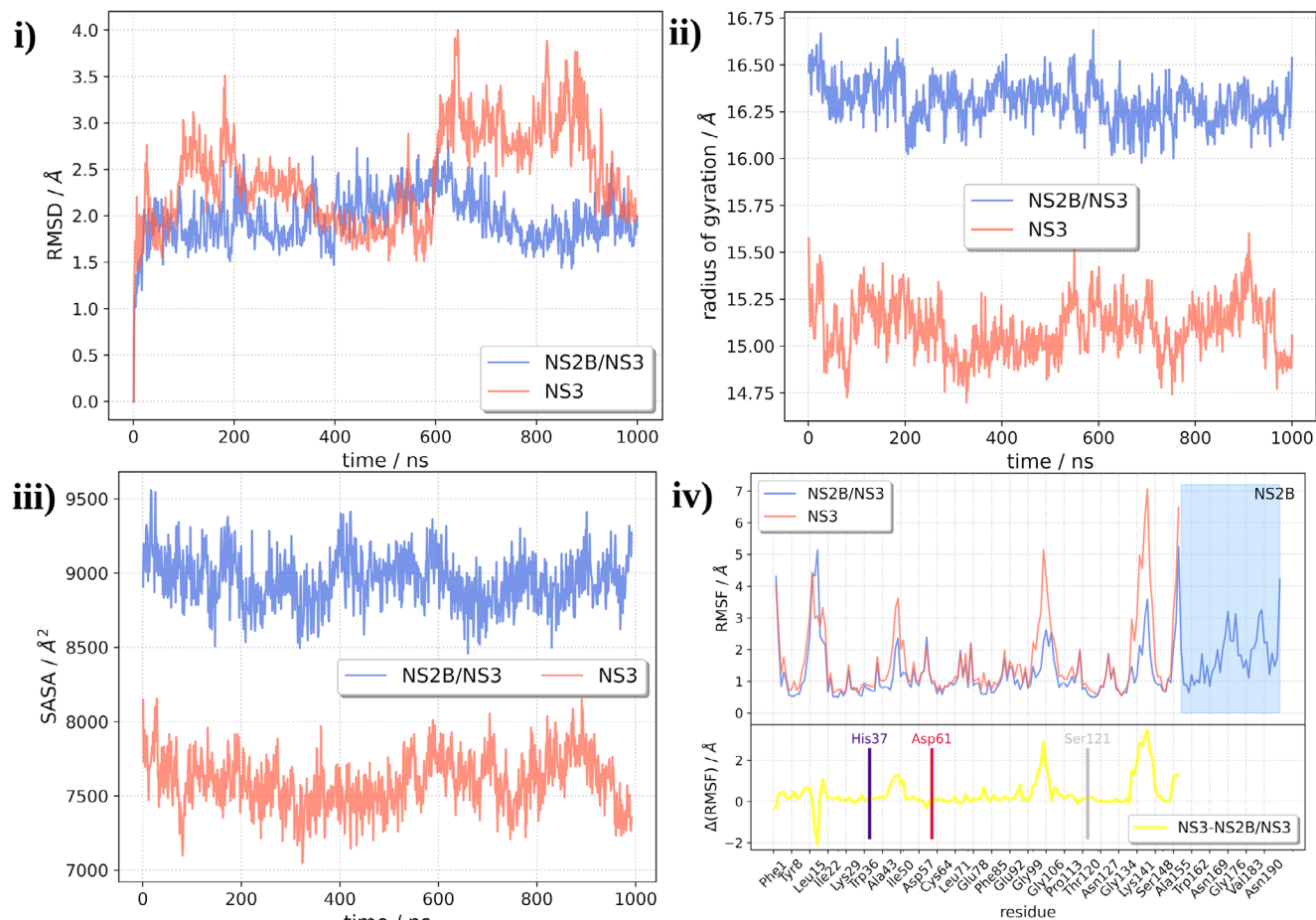
**ADVANCED
SCIENCE NEWS**

www.advancedsciencenews.com

**ADVANCED
THEORY AND
SIMULATIONS**

www.advtheorysimul.com

Figure 1. MD trajectory analysis comparing NS2B/NS3 and NS3 protease: i) Backbone RMSD, ii) Radius of gyration, iii) Solvent accessible surface area, and iv) Root mean square fluctuations per residue (upper panel) and the difference of RMSF values between free NS3 protein and NS2B-complexed NS3 protein (lower panel).

Table 1. Statistical analysis of molecular dynamics simulations for the apo forms of NS2B/NS3 and NS3 protease.

Protein	RMSD [Å]	RoG [Å]	SASA [Å^2]	RMSF [Å]
NS3	2.42 ± 0.51	13.3 ± 0.1	7594 ± 180	1.64 ± 1.21
NS2B/NS3	1.97 ± 0.26	15.1 ± 0.1	8953 ± 173	1.36 ± 0.87

Table 2. Contributions of the most important residues in NS2B/NS3 binding.

NS2B residues	ΔG_{bind} [kcal mol^{-1}]	NS3 residues	ΔG_{bind} [kcal mol^{-1}]
Leu158	-8.6 ± 0.3	Tyr8	-4.9 ± 0.1
Trp162	-8.4 ± 0.4	Val45	-4.5 ± 0.1
Trp168	-8.2 ± 0.2	Ile102	-4.4 ± 0.5
Ile159	-7.2 ± 0.2	Gln81	-4.2 ± 0.2
Ala160	-5.5 ± 0.1	Tyr11	-4.1 ± 0.2
Val166	-5.4 ± 0.3	Leu140	-3.9 ± 0.2

Gly106, and Asn138-Tyr146 demonstrate ΔRMSF values more than twice the mean (0.38 Å), while ΔRMSF of Leu16 and Trp17 is notably below –0.75 Å. Residues constituting the catalytic triad, His37, Asp61, and Ser121, exhibit RMSF and ΔRMSF values below the average.

In addition to structural analysis, the binding free energy of NS2B to NS3 was estimated. The 1 μs trajectory was divided into 20 segments of 50 ns each, and the free energy of binding was calculated for each segment using the MM/GBSA method. Reported values represent the average and standard deviation across all 20 segments. Due to computational constraints, entropy contributions were not calculated. The binding free energy is determined to be -164.7 ± 6.0 kcal mol^{-1}, with contributions from van der

Waals, electrostatic, and nonpolar solvation energies of –216 kcal mol^{-1}, 255 kcal mol^{-1}, and –27 kcal mol^{-1}, respectively.

Per-residue energy decomposition was conducted to ascertain the contribution of both NS2B and NS3 residues to NS2B binding. In **Table 2**, the top six residues along with their corresponding contributions to the total free energy of binding are compiled. Notably, residues from the *N*-terminal side of NS2B, including Leu158 (–8.6 kcal mol^{-1}), Ile159 (–7.2 kcal mol^{-1}), Ala160 (–5.5 kcal mol^{-1}), and Trp162 (–8.4 kcal mol^{-1}), alongside Trp168 (–8.2

**ADVANCED
SCIENCE NEWS**

www.advancedsciencenews.com

**ADVANCED
THEORY AND
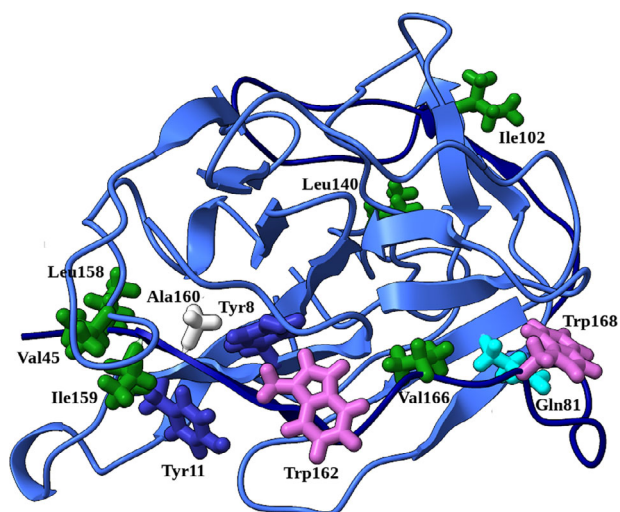SIMULATIONS**

www.advtheorysimul.com

Figure 2. The most important residues in NS2B/NS3 binding. Isoleucine, leucine and valine are depicted in green, alanine in white, tyrosine in dark blue, and tryptophan in violet.

Table 3. Analysis of active pocket of NS2B/NS3 (His37$^+$/Asp61$^-$/Ser121$^-$) and NS2B/NS3 (His37^0/Asp61$^-$/Ser121^0).

Complex	Volume [Å^3]	Buriedness
NS2B/NS3:A (His37^0/Asp61$^-$/Ser121^0)	507.4	0.746
NS2B/NS3:B (His37^0/Asp61$^-$/Ser121^0)	623.4	0.676
NS2B/NS3:A (His37$^+$/Asp61$^-$/Ser121$^-$)	636.7	0.734
NS2B/NS3:B (His37$^+$/Asp61$^-$/Ser121$^-$)	618.3	0.669

Table 4. k-means cluster analysis of NS2B/NS3 binding pocket.

Cluster	Conformation	Cluster Population	d[a]	csd[b]	RMSD against A[c]
1	**A**	0.374	1.837	0.338	0
2	**B**	0.295	1.715	0.288	0.668
3	**C**	0.280	1.920	0.361	0.494
4	**D**	0.051	1.798	0.252	1.111

[a]Average distance between points in the cluster, [b]Standard deviation of points in the cluster, [c]in Å

kcal mol^{-1}), emerge as pivotal. From the perspective of NS3, Tyr8 (−4.9 kcal mol^{-1}) and Val45 (−4.5 kcal mol^{-1}) are identified as key residues for cofactor binding. As depicted in **Figure 2**, there is a clustering of residues with similar properties, wherein Leu159 and Ile160 of NS2B engage in nonpolar interactions with Val45 of NS3. Additionally, an intriguing π-π interaction is observed between the indole ring of Trp168 and the amide group of Gln81 side chain.

Additionally, we compared the NS2B/NS3 (His37$^+$/Asp61$^-$/Ser121$^-$) and NS2B/NS3 (His37^0/Asp61$^-$/Ser121^0) systems to understand the structural changes that occur in the active site. It is well established that in serine proteases, the catalytic triad–comprising histidine, serine, and aspartate–works in concert to enhance nucleophilicity and facilitate substrate cleavage. The selection of neutral His37, neutral Ser121, and deprotonated Asp61 is physiologically relevant, as the neutral histidine effectively functions as a proton shuttle, facilitating proton transfer during catalysis. The neutral state of serine ensures it remains primed for activation by histidine, enabling a nucleophilic attack on the substrate, while the deprotonated aspartate stabilizes the positively charged histidine, promoting proper alignment and enhancing catalytic efficiency.[23] This nucleophilic nature of the catalytic serine has been exploited in the development of first-generation inhibitors (telaprevir, boceprevir, and narlaprevir) against HCV NS3/4A protease. Hence, a comparison of the protonation state of the active pocket amino acids is conducted to understand structural changes.[24] To this end, the representative structures of the two most populated clusters from both systems were considered for comparison. We observed a key difference: in the NS2B/NS3 (His37^0/Asp61$^-$/Ser121^0) system, the formation of the oxyanion hole is not as pronounced, and the oxygen of the active site serine points downward (serine is mainly responsible for the formation of the oxyanion hole). However, in the NS2B/NS3 (His37$^+$/Asp61$^-$/Ser121$^-$) system, the formation of the oxyanion hole is much clearer, as depicted in Figure S3 (Supporting Information). Hence, it is crucial to

consider the protonation state of the active site amino acid when developing new inhibitors through in silico approaches. Along with that, the active site volume, and buriedness of the two systems were also measured (**Table 3**). The volume of the active pocket in the two systems was found to be almost the same. However, some changes were observed in cluster A of the NS2B/NS3 (His37$^+$/Asp61$^-$/Ser121$^-$) system. Additionally, the buriedness of the active pocket was measured for both systems, with values ranging between 0.6 and 0.7, indicating a partially buried surface area.

2.3. NS2B/NS3 Clustering

The k-means cluster analysis based on the RMSD of Cα atoms was utilized to identify distinct conformations within the active pocket of the NS2B/NS3 protease. This approach aims to enhance the likelihood of a successful virtual screening campaign. We examined all k values ranging from 2 to 5 to determine the optimal number of conformations, and the outcomes were assessed using the Davies–Bouldin index (DBI), pseudo-F statistic (pSF), and ratio of sum of squares of the regression to the sum of squares error (SSR/SST) (Table S1, Supporting Information). The DBI evaluates the compactness and separation of clusters, where lower values indicate better clustering. The pSF measures the ratio of between-cluster variance to within-cluster variance, with higher values signaling more distinct clusters. The SSR/SST ratio quantifies the proportion of variance explained by the clustering, with higher values indicating a better fit of the data. These three metrics were collectively used to ensure the robustness of the optimal clustering solution. The presence of four significant conformations was confirmed (**Table 4**). The structure nearest to the centroid of the cluster was selected as the representative structure for each conformation.

When comparing the active pocket residues in the two most populated conformations (**A** and **B**), several noteworthy observations emerged (**Figure 3**). First, the relative positions of catalytic residues remained highly conserved. Second, the side chain of
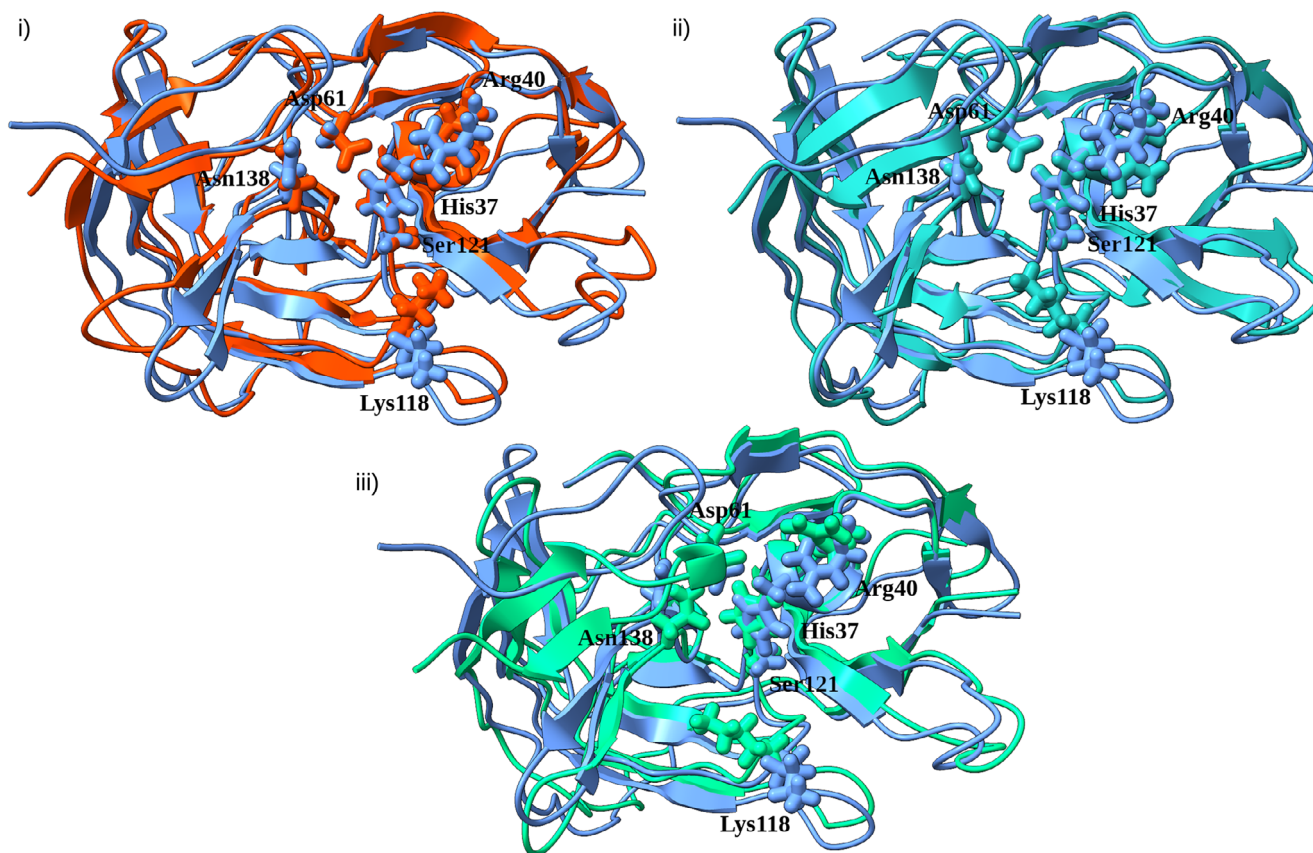
ADVANCED
SCIENCE NEWS

www.advancedsciencenews.com

ADVANCED
THEORY AND
SIMULATIONS

www.advtheorysimul.com

Figure 3. NS2B/NS3 active pocket conformation comparison. Conformers **B** (orange red, i), **C** (sea green, ii), and **D** (spring green, iii) overlaid with conformer **A** (blue).

Lys118 exhibited a notable movement towards His37 and Arg40 residues, resulting in a reduction in the pocket's volume and potentially impeding substrate accessibility to the binding site. Similar conclusions can be drawn for conformation **C**, albeit with minor additional reorientation of the Arg40 side chain. Conversely, the least populated **D** conformation (5.1%) demonstrated the most significant changes in active pocket residues, with only the relative orientation of Asp61 and Ser121 being conserved.
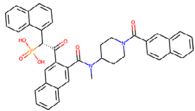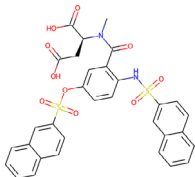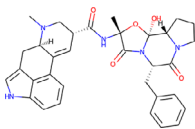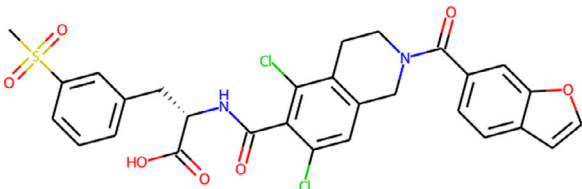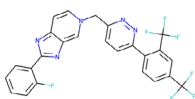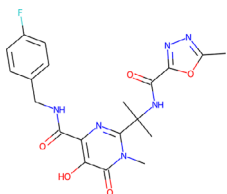
2.4. Drug Repurposing

A total of 9288 molecules sourced from the DrugBank database underwent docking against four distinct conformations of the NS2B/NS3 protease, each characterized by a unique geometry of the active pocket. Given that these molecules are either approved drugs or in various stages of clinical trials, it is assumed that their ADMET properties meet the standards for drug candidacy. The conformation-averaged docking score was computed using Equation 1, yielding an averaged score for the best docking pose of -6.52 ± 0.96 kcal mol^{-1}. Supporting Information includes a CSV document listing all docked compounds, their scores for each conformation, and the total averaged score. Additionally, **Table 5** presents the 2D structures and docking scores of six drugs selected for all-atom molecular dynamics simulations. Figures S4–S7 (Supporting Information) illustrate the interac-

tion diagram of the hit molecules with conformations **A–D** of Alkhumra's NS2B/NS3 protease for the docked poses. Table S2 (Supporting Information) presents the interactions observed in docked ligands across four conformations of the NS2B/NS3 complex.

Due to computational limitations, our selection strategy prioritized molecules with the highest binding potential, comprising two compounds with the most favorable binding scores, along with two approved drugs and two antiviral agents demonstrating the best averaged docking scores. Notably, DB12983 emerged with the highest averaged docking score. However, as phthalocyanine, an organoheterocyclic tetrapyrrole, has previously undergone clinical trials as part of photodynamic therapy (ClinicalTrials.gov Identifier NCT00103246, accessed on April 12, 2024), it was excluded from our list of hit molecules. Experimental drugs DB04016 and DB01879, although slightly lower in score compared to DB12983, were included. Additionally, approved drugs DB00696 and DB11611 exhibited averaged docking scores below -9 kcal mol^{-1}. Finally, the antiviral agents Tegobuvir (DB11852) and Raltegravir (DB06817) ranked highest among their category.

The initial structures for molecular dynamics simulations were obtained by docking DrugBank molecules with the highest score to the NS2B/NS3 protease. Due to limited computational resources, molecular dynamics simulations were conducted for all six selected drugs bound to the highest populated conformation (**A**). All simulations were performed in triplicates to ensure

**ADVANCED
SCIENCE NEWS**

www.advancedsciencenews.com

**ADVANCED
THEORY AND
SIMULATIONS**

www.advtheorysimul.com

Table 5. Molecular docking results of six hit molecules to NS2B/NS3 binding pocket.

DrugBank ID	2D structure	A	B	C	D	K_w
DB04016		−10.209	−9.132	−8.966	−8.698	−9.466
DB01879		−9.658	−9.531	−8.811	−9.492	−9.375
DB00696		−9.765	−10.197	−7.668	−7.345	−9.186
DB11611		−9.617	−8.725	−8.703	−7.827	−9.007
DB11852		−8.499	−8.684	−8.092	−7.985	−8.413
DB06817		−8.107	−8.428	−8.701	−7.199	−8.321

statistical reliability. Among these, only three drugs (DB01879, DB04016, and DB11611) remained within the protease active pocket for the entire 150 ns simulation period in all three triplicates. The results for these three drugs are presented in the main text (**Figure** 4, with additional analysis for all triplicates in Figures S8–S10, S16, S17, and S20, Supporting Information), while the analysis of the other drugs is provided in the Supporting Information (Figures S11–S15, S18, S19, and S21, Supporting Information). Since DB00696, DB06817, and DB11852 moved out of the catalytic pocket in at least one of the triplicates, they were removed from the list of potential competitive inhibitors of Alkhumra's NS2B/NS3 protease.

The complexes formed by DB01879, DB04016, and DB11611 with the NS2B/NS3 protease were observed to exhibit stability, characterized by minimal fluctuations in the protein's backbone Cα atoms when compared to the initial structures. Additional stability parameters, including radius of gyration, solvent-accessible surface area (SASA), and root-mean-square fluctuation (RMSF), are detailed in Figures S8–S10 and Table S3 (Supporting Infor-

mation). Analysis of these metrics indicates that these complexes maintain stability, with dominant conformation. The RMSD values of Cα atoms of the protein backbone for the three stable complexes are notably low, with mean values below 1.55 Å. The RMSD of ligands is mostly below 2 Å for DB04016 and DB11611, and around 3 Å for DB01879. Higher flexibility within the catalytic pocket is expected for DB01879 due to its higher number of rotatable bonds (11) compared to DB04016 (7) and DB11611 (7). We further examined the distance between the center of mass of the ligands and the CG atom of His37 and the OG atom of Ser121 (Table S4). DB01879 and DB04016 are in average for 0.5 Å closer to His37 than DB11611, with higher standard deviation. DB01879 is also significantly closer to Ser121, in average 5.74 Å. DB11611 has almost one and half the distance (8.61 Å). Visualization of MD trajectory offers explanation of observed differences. While DB01879 is positioned between Ser121 and Lys118 side chain, Lys118 side chain is between DB11611 and Ser121, pushing drug away. Although drugs have different binding poses, access to catalytic residues is blocked. A deeper insight into the
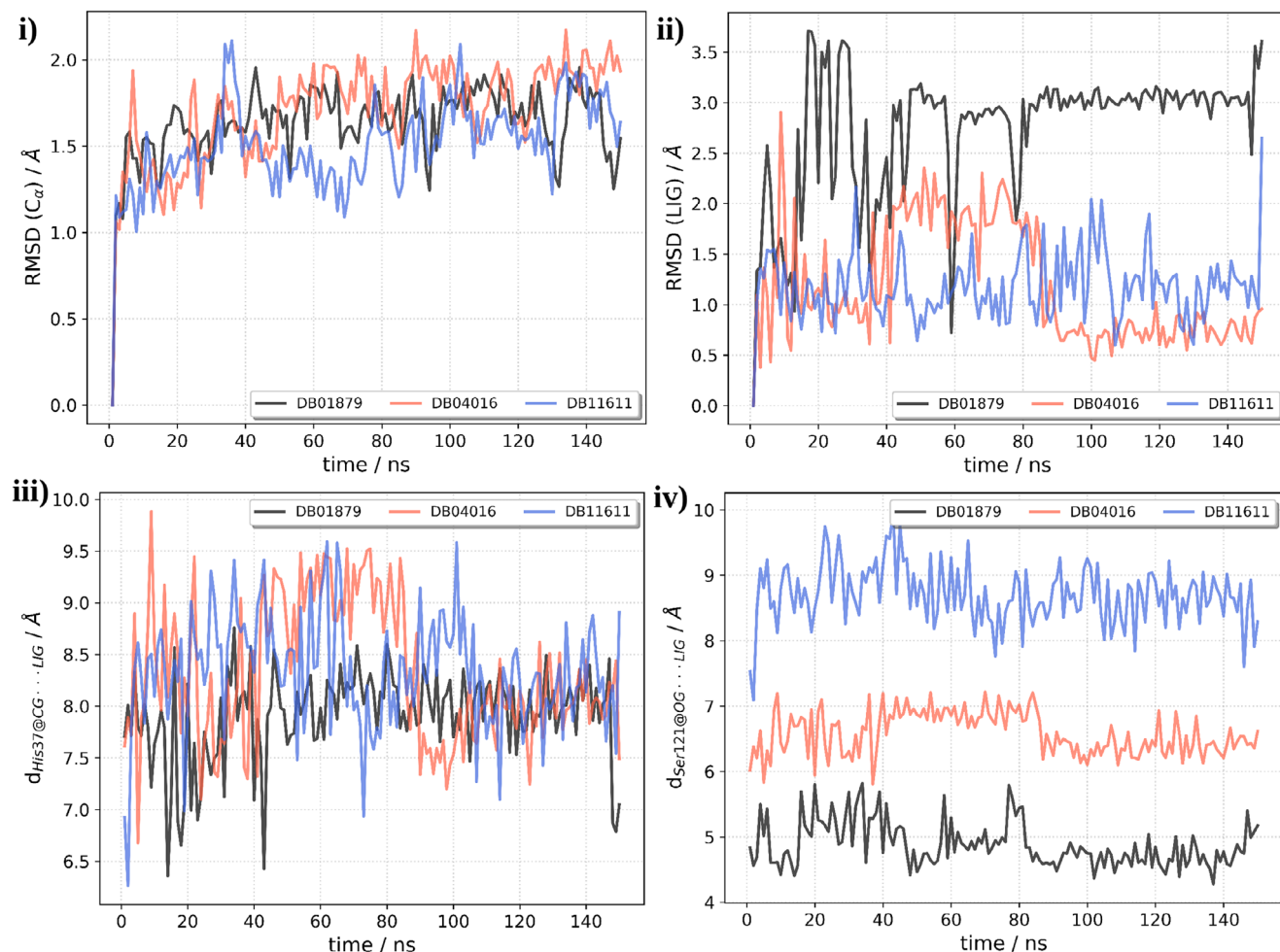
ADVANCED
SCIENCE NEWS
www.advancedsciencenews.com

ADVANCED
THEORY AND
SIMULATIONS
www.advtheorysimul.com

Figure 4. Analysis of molecular dynamics simulations of NS2B/NS3:ligand complexes. Root mean square deviation of NS2B/NS3 Cα atoms (i) and of ligand (ii), distance between the center of mass of ligand and His37 CG atom (iii), and Ser121 OG atom (iv).

influence of ligands on the catalytic triad residues was obtained by analyzing the relative distances between the side chains of Ser121, His37, and Asp61 (Figures S16–S10 and Table S5, Supporting Information). For most ligands, these distances remain relatively stable throughout the simulation, suggesting that the catalytic triad maintains its structural integrity in their presence. However, certain ligands, such as DB01879 and DB11611, induce notable fluctuations, including transient spikes in the distances. The mean Ser121 OG ⋯ His37 CG distances are comparable across all complexes, with a maximum standard deviation below 4%, indicating minimal disruption of this key interaction. In contrast, the mean Ser121 OG ⋯ Asp61 CG distances exhibit greater variability, with the NS2B/NS3 protease complexed with DB01879 showing the largest average distance (8.15 Å). These findings suggest that while most ligands do not significantly alter the catalytic triad's relative positioning, certain compounds may induce dynamic perturbations that could influence enzymatic function.

The single trajectory approach MM/GBSA was utilized to estimate the free energy of ligand binding to the NS2B/NS3 protease. This method has been widely and successfully employed in studies of protein-ligand interactions, particularly for Flavivirus

proteases, where it has provided reliable estimates of binding free energies. Notably, MM/GBSA has been applied to NS2B/NS3 proteases of related viruses, including Kyasanur forest disease virus,[22] Zika,[25,26] and dengue,[27] consistently producing results that align with experimental observations.[28] Studies by Mirza et al.,[29] Rehman et al.,[30] and Cruz-Arreola et al.[31] have demonstrated the robustness of MM/GBSA through successful identification and validation of Zika and dengue protease inhibitors using molecular dynamics simulations and high-throughput screening. These studies underscore the robustness and reliability of the MM/GBSA approach for examining binding free energies in systems closely related to our target, even in cases where experimental validation is not feasible. Values presented in **Table 6** represent mean values with standard deviations calculated from three 50-ns MD trajectory segments. Among the compounds, DB04016 exhibited the most favorable free energy of binding, devoid of unfavorable entropic contributions. Both DB01879 and DB04016 showed a predominant contribution from electrostatic interactions, whereas DB11611 exhibited the lowest nonpolar contribution to solvation. Electrostatic contributions to solvation and van der Waals energy were found to be similar for all three drugs. Although electrostatic

2401406 (7 of 13)

**ADVANCED
SCIENCE NEWS**

www.advancedsciencenews.com

**ADVANCED
THEORY AND
SIMULATIONS**

www.advtheorysimul.com

Table 6. Energy analysis for the binding of DB01879, DB04016, and DB11611 to Alkhumra NS2B/NS3 protease as obtained by MM/GBSA method. All values are reported in kcal mol^{-1}.

Ligand	ΔE_{vdW}[a]	$\Delta E_{electrostatic}$[b]	ΔE_{MM}[c]	ΔG_{SA}[d]	ΔG_{GB}[e]	ΔG_{bind}[f]
DB01879	-38.9 ± 2.8	-71.6 ± 15.7	-110.5 ± 18.3	-5.2 ± 0.4	75.3 ± 14.1	-40.5 ± 4.8
DB04016	-38.0 ± 1.9	-83.7 ± 2.9	-121.7 ± 3.8	-5.4 ± 0.2	75.7 ± 2.6	-51.4 ± 2.0
DB11611	-41.2 ± 6.9	-36.5 ± 5.1	-77.8 ± 11.7	-4.8 ± 0.7	55.1 ± 6.0	-27.6 ± 7.5

[a]van der Waals energy, [b]electrostatic energy, [c]electrostatic + van der Waals energy, [d]electrostatic contribution to solvation, [e]nonpolar contribution to solvation, [f]free energy of binding without entropy contribution.

Table 7. Contributions of the most important amino acid residues for the binding of DB01879, DB04016, and DB11611 to Alkhumra NS2B/NS3 protease. All values are reported in kcal mol^{-1}.

DB01879		DB04016		DB11611	
Residue	ΔG_{bind}	Residue	ΔG_{bind}	Residue	ΔG_{bind}
Ser121	-6.9 ± 1.2	Ser121	-11.0 ± 0.6	Tyr146	-3.2 ± 1.3
Lys118	-3.7 ± 0.4	Lys118	-3.8 ± 0.1	Lys141	-1.6 ± 0.4
Tyr146	-2.4 ± 0.3	Tyr146	-2.1 ± 0.2	Gly139	-1.6 ± 0.7
His37	-1.6 ± 0.8	Gly119	-1.6 ± 0.1	His37	-1.5 ± 1.0
Gly119	-1.5 ± 0.2	Lys141	-1.4 ± 0.4	Lys118	-1.4 ± 0.3

interactions between DB01879 and DB04016 and NS2B/NS3 were deemed crucial, the significance of intramolecular hydrogen bonding should not be overlooked (Figures S20 and S21, Supporting Information).Energy decomposition analysis provides insights into the nature of interactions between the ligand and individual residues, such as hydrogen bonding, van der Waals interactions, electrostatic interactions, and hydrophobic interactions. Indeed, energy decomposition per residue analysis supports our MM/GBSA and hydrogen bond conclusions. **Table 7** lists the amino acid residues that contribute the most to the free energy of binding. In the cases of DB01879 and DB04016, which form strong and long-lasting hydrogen bonds with Ser121, Ser121 is identified as the most contributing residue. The magnitude of the ΔG_{bind} contribution suggests a strong electrostatic role. Following Ser121, Lys118, a residue with a positively charged side chain, is prominent. The hydroxyphenyl moiety of Tyr146 can form a hydrogen bond and $\pi-\pi$ interactions with one of the aromatic rings of the ligands. DB11611 adopts a different pose within the pocket, resulting in a different binding pattern. Nonetheless, charged residues (Lys141 and Lys118), hydrophobic residues (Tyr146 and Leu140), and neutral but polar residue (His37) play dominant roles.

3. Discussion

The analysis of MD trajectories allow us to draw several important conclusions. RMSD serves as a common metric for assessing structural disparity between coordinates. It quantifies the typical displacement among a set of atoms (e.g., backbone atoms within a protein). When computing RMSD between two sets of atomic coordinates, such as two time points within a trajectory, the resulting value indicates the degree of alteration in the protein's conformation. The low mean RMSD values (below 2.5 Å) of proteins' backbone atoms suggest that conformation is stable. Addi-

tionally, the low standard deviation for NS2B/NS3 suggests minimal conformational changes during dynamics, contrasting with the RMSD fluctuations seen in free NS3, which indicate greater flexibility. The effect is even more pronounced when considering RMSD solely for NS3 within the NS2B/NS3 protease, yielding an RMSD of 1.25 ± 0.85 Å.

The stability is further supported by RoG and SASA analyses, which exhibit minor fluctuations around their mean values. Visual inspection of the overlaid first and last structures from MD simulations reveals minimal structural alterations (see Figure S22, Supporting Information). These alterations primarily involve flexible unstructured loops and are more prominent in the case of the free NS3 protein. Additionally, the secondary structure remains conserved throughout the MD simulation (see Figure S23, Supporting Information).

The RMSF analysis provides insights into the impact of NS2B cofactor binding on the flexibility of the NS3 protease. Generally, the binding of the NS2B cofactor reduces the overall flexibility of NS3, while having minimal effect on the flexibility of catalytic residues. Three distinct regions of NS3, which exhibit significantly reduced flexibility upon NS2B cofactor binding, are identified (refer to Figure S24, Supporting Information). Notably, the regions experiencing reduced flexibility are in direct contact with the NS2B cofactor. Specifically, the regions encompassing residues Val45-Ile50 and Leu16-Trp17 demonstrate increased flexibility at the N-terminus of NS3. Conversely, residues Glu100-Gly106 form a parallel β-sheet motif with the NS2B cofactor, indicating a stabilized interaction interface. Additionally, residues Asn138-Tyr146 constitute an unstructured loop that encloses the β-sheet motif from the opposite side. Remarkably, similar patterns of flexibility alteration were observed in the NS2B/NS3 protease complex of the KFDV.[22] These findings suggest that the binding of the NS2B cofactor induces localized structural changes in the NS3 protease, resulting in altered flexibility patterns within specific regions of the protein. Such alterations may play a pivotal role in modulating the enzymatic activity and substrate recognition of the NS3 protease complex.

The free energy of binding analysis demonstrates a high affinity for the binding of the NS2B cofactor to the NS3 protease. Further decomposition of the free energy reveals the significance of nonbonding van der Waals interactions and electrostatic interactions in the bonding process. A deeper analysis confirms these findings by highlighting the dominant contribution of hydrophobic residues from both chains to the free energy of binding. In addition to van der Waals interactions, residues such as tyrosine and tryptophan may be involved in hydrogen bond formation, as well as in $\pi-\pi$ interactions, which provide additional stabilization to the complex. These interactions collectively contribute to

the overall stability of the NS2B cofactor–NS3 protease complex, enhancing its affinity and facilitating efficient binding.

NS2B is an integral membrane protein weighing 14 kDa and comprising three domains. Among these domains, the central one, a 47-amino-acid segment, acts as an essential cofactor for the NS3 protease, while the other two domains are transmembrane regions located at the *C* and *N* terminal regions.[32] The *β*-hairpin structure formed by the central core domain of NS2B plays a crucial role in completing the active substrate binding site within the NS3 protease. This structural formation significantly contributes to the creation of the hydrophobic S2 and S3 pockets, directly influencing catalysis.[33,34] Previous studies have unequivocally demonstrated that in vitro, the Flavivirus NS3 protein exhibits incorrect folding, leading to insolubility and a lack of catalytic activity as a protease in the absence of NS2B.[35] Also, evident from previous crystal structures of Flavivirus NS2B/NS3 protease that the protease can adopt two distinct conformations—"opened" and "closed." These variations in conformation stem from the orientation of NS2B within the active pocket.[36] Therefore, NS2B-induced conformational changes are crucial for NS3 function.

The changes in the protonation states of the active site amino acids were done to mimic exact enzyme catalysis. The general enzyme catalysis of serine protease is as follows: The canonical His–Asp–Ser catalytic triad follows the general acyl transfer mechanism of serine proteases. The catalytic histidine and aspartic acid increase the nucleophilicity of the serine, thereby increasing the reaction rate with the scissile carbonyl carbon of the substrate. The deprotonated serine hydroxyl attacks the carbonyl carbon of the substrate, generating an acylated tetrahedral intermediate. The high-energy intermediate is stabilized by the oxyanion hole composed of the backbone amide nitrogen atom and the Nε of the catalytic histidine. The scissile amide nitrogen is then protonated by histidine, generating a new *N*-terminus and leaving an ester acylated protease that is hydrolyzed by a water molecule to generate a new *C*-terminus, completing the catalytic cycle.[24] Hence, we prepared the system in both His37$^+$/Asp61$^-$/Ser121$^-$ and His37^0/Asp61$^-$/Ser121^0 protonation states and compared the structural changes that occur in the active site.

Our selection of hit drugs comprises six compounds, chosen based on their averaged docking scores. Among them, DB04016 and DB01879 are experimental drugs with limited information available regarding their targets and mechanisms of action. Ergotamine (DB00696) functions as an alpha-1 selective adrenergic agonist vasoconstrictor, primarily prescribed for the treatment of migraines.[37] Lifitegrast (DB11611) is an FDA-approved medication indicated for managing keratoconjunctivitis sicca (dry eye syndrome).[38] Tegobuvir (DB11852) has garnered attention for its potent antiviral activity against HCV, believed to stem from its binding to an allosteric site in the NS5B polymerase.[39] Raltegravir (DB06817) functions by inhibiting HIV integrase, thereby preventing the integration of the viral genome into the human genome.[40]

Both antiviral drugs failed to form stable complexes with Alkhurma's NS2B/NS3 protease in at least one of the triplicates. DB11852 initially resided within the active pocket of conformation **A** for the first 45 ns before transiently moving away. It returned for an additional 30 ns before finally dissociating. Similarly, DB06817 rapidly dissociated from NS2B/NS3 after 15 ns,

and DB00696 within 10 ns. These findings underscore the disparity between static molecular docking experiments and the dynamic binding capabilities observed in molecular dynamics simulations. Moreover, they raise questions regarding the suitability of the NS2B/NS3 protease active pocket for noncovalent inhibitor design, given its flat and shallow geometry and highly charged surroundings, including protonated His37, and deprotonated Asp61 and Ser121.

The difference in hydrogen bond patterns between stable and unstable NS2B/NS3:ligand complexes may account for ligands drifting away from the catalytic pocket in unstable complexes. By comparing the evolution of hydrogen bonds (Figures S20 and S21, Supporting Information), one can observe a higher hydrogen bond count for stable complexes. Statistical analysis supports this observation: DB01879, DB04016, and DB11611 exhibit an average of 2.9, 3.5, and 1.8 hydrogen bonds, respectively, whereas DB00696, DB06817, and DB11852 show 0.9, 1.2, and 0.2 hydrogen bonds, respectively. Another significant finding is that both DB01879 and DB04016 form hydrogen bonds with Ser121, persisting throughout 99% of the simulation time (**Figure 5**). These hydrogen bonds likely contribute to the overall stability of the protein–ligand complexes by anchoring the ligands in the binding pocket. This stabilizing effect could enhance the residence time of the ligands within the pocket, increasing the likelihood of effective inhibition of the target protein. Additionally, the formation of hydrogen bonds may induce conformational changes in the protein, leading to allosteric effects that further stabilize the complex or modulate its activity. Energy decomposition per residue after MM/GBSA calculation of free energy of binding is performed to understand the contributions of individual amino acid residues to the overall binding affinity between a ligand and its target protein. This analysis helps identify key interactions between the ligand and specific residues within the binding site, shedding light on the molecular basis of ligand–protein recognition and binding. This information is valuable for structure-based drug design as it identifies "hotspot" residues that are crucial for ligand binding. These residues can then be targeted for optimization to enhance binding affinity and selectivity. Key residues for binding (**Figure 6**), such as charged residues such as Ser121, His37, Lys118, and Lys141, as well as hydrophobic residues (Tyr146, Gly119), have been identified. The dominance of charged residues, particularly the high contribution of Ser121, corroborates the MM/GBSA free energy of binding calculations and the dominance of electrostatic energy contributions. DB11611 is farthest from Ser121, and Ser121 does not play a significant role in its binding. This is also reflected in the electrostatic energy contribution, with a magnitude significantly smaller compared to DB01879 and DB04016.

4. Conclusions

The analysis of MD trajectories provides several important insights. RMSD analysis indicates that the conformation of the NS2B/NS3 complex is stable, with low mean RMSD values below 2.5 Å, contrasting with the higher flexibility observed in free NS3. The stability is further supported by RoG and SASA analyses, with minor fluctuations observed around their mean values. Visual inspection of the structures reveals minimal structural alterations, primarily in flexible loops, and conservation of secondary
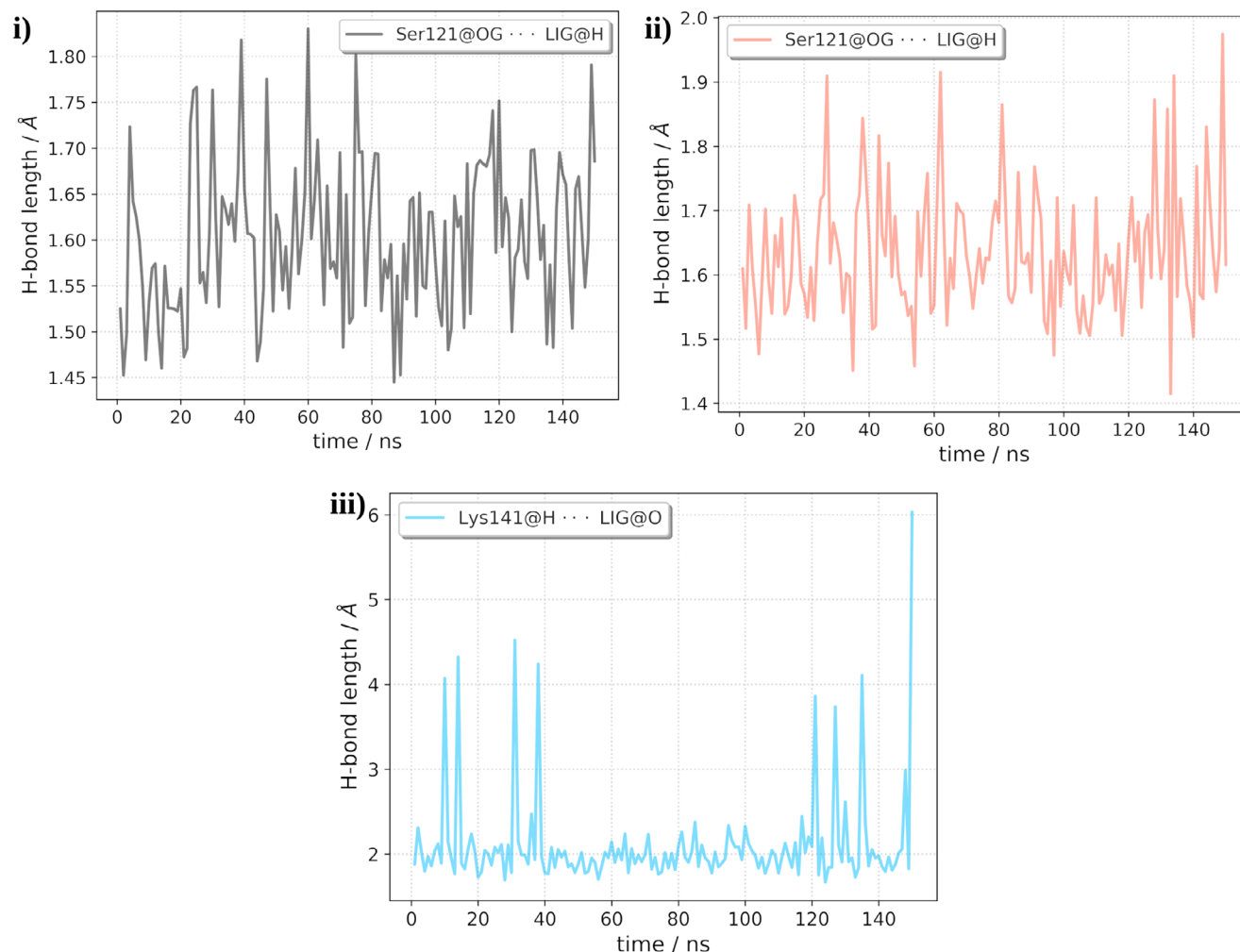
**ADVANCED
SCIENCE NEWS**

www.advancedsciencenews.com

**ADVANCED
THEORY AND
SIMULATIONS**

www.advtheorysimul.com

Figure 5. Dominant hydrogen bond length between ligands and NS2B/NS3. DB01879 (i), DB04016 (ii), and DB11611 (iii).

structure throughout the simulations. Additionally, RMSF analysis highlights the role of the NS2B cofactor in reducing NS3 flexibility, particularly in regions in contact with NS2B. Moreover, per-residue energy decomposition analysis underscores the importance of nonbonding van der Waals interactions and electrostatic interactions in the binding process.

Over 9000 compounds from the DrugBank database underwent docking to four conformations of the NS2B/NS3 protease catalytic pocket, resulting in the selection of two experimental, two FDA-approved drugs, and two antiviral agents for further molecular dynamics simulations. The difference in hydrogen bond patterns between stable and unstable complexes, particularly the persistent hydrogen bonds formed by DB01879 and DB04016 with Ser121, suggests a stabilizing effect that enhances the residence time of the ligands in the binding pocket. Energy decomposition per residue analysis further confirms the role of specific residues in binding, with charged residues dominating the contributions. This comprehensive analysis sheds light on the molecular interactions underlying ligand binding to NS2B/NS3, providing valuable insights for the development of effective inhibitors.

5. Experimental Section

Generating the 3D Structure of the ALKV NS2B/NS3 Protease: The annotated protein sequence of the NS2B/NS3 protease of ALKV was retrieved from the NCBI Gene Bank (accession ID AAL08421.1).[41] The amino acid region in the polyprotein from 1381 to 1671 was selected for structure prediction using AlphaFold. Both the *N*- and *C*-termini of NS2B, which consist of transmembrane domains, were removed, leaving only the cytoplasmic loop, which is essential for the interaction with NS3 and acts as a cofactor in the protease activity. Structure prediction was conducted using the AlphaFold source code in the Google Colab notebook accessible through a portal hosted by the European Bioinformatics Institute (http://alphafold.ebi.ac.uk , accessed on December 29, 2022). The residues of the final model were renumbered from 1 to 156 for NS3 and from 157 to 195 for NS2B, for convenience in the present work.

Molecular Dynamics (MD) Simulation of NS2B/NS3 and NS3 Proteins: MD simulations were conducted using the AMBER22 program[42] to model the NS3 protease with and without the NS2B cofactor. The simulation protocol was adapted from a previous study,[22] with the main modification being an extended productive simulation duration of 1000 ns, while maintaining consistent parameters such as periodic boundary conditions, NVT conditions, pressure, and temperature.

The simulations were carried out in two sequential steps: energy minimization, followed by equilibration and production runs. To remove steric
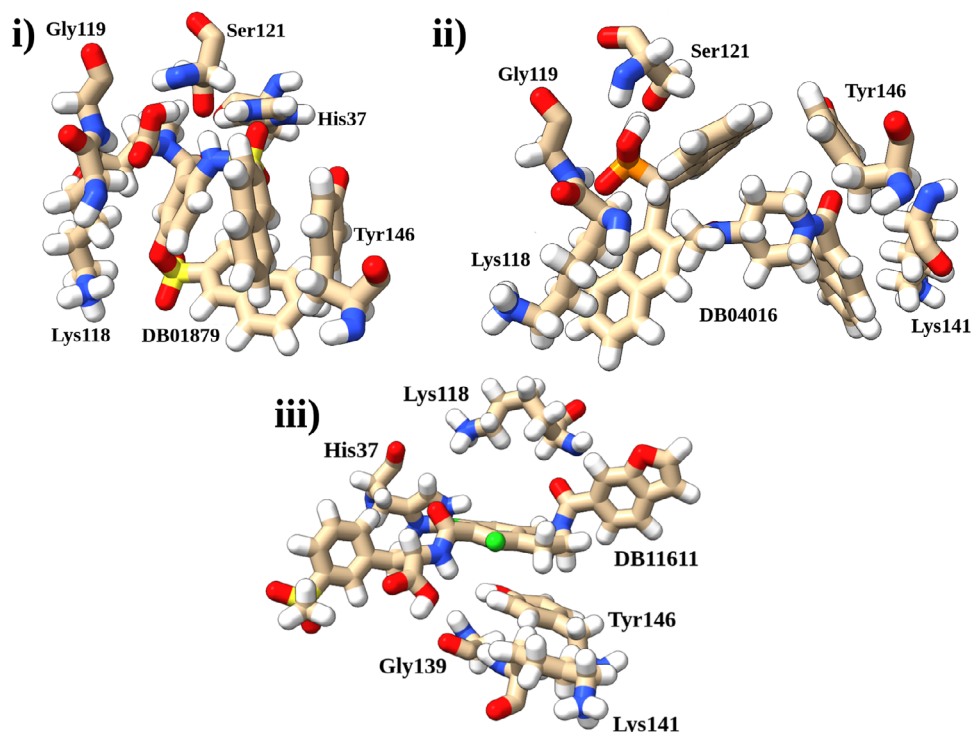
Figure 6. Ligands in the active pocket of NS2B/NS3 protease. DB01879 (i), DB04016 (ii), and DB11611 (iii).

clashes and optimize the system before the MD simulations, a two-step energy minimization protocol was applied. In the first step, the complex was restrained (force constant = 10.0 kcal mol^{-1} Å^{-2}), allowing only the water molecules to be optimized. This step consisted of 4000 cycles of the steepest descent method, followed by 6000 cycles of the conjugate gradient method, totaling 10 000 cycles. In the second step, the restraints were removed, and both the protein and water molecules were minimized using 4000 cycles of the steepest descent method, followed by 6000 cycles of the conjugate gradient method.

The minimized systems were gradually heated from 0 to 310 K over 500 ps under the canonical ensemble (NVT conditions). The production MD simulations were then conducted for 1000 ns using a time step of 2 fs under isothermal-isobaric (NPT) conditions, maintaining a constant temperature of 310 K and a pressure of 1 atm. Temperature control was achieved using a Langevin thermostat with a collision frequency of 1 ps^{-1}. Bond constraints involving hydrogen atoms were applied using the SHAKE algorithm. Long-range electrostatic interactions were computed using the Particle Mesh Ewald method, while non-bonded interactions were truncated at a cutoff distance of 11.0 Å.

The AMBER ff19SB force field was employed for system parametrization. Prior to simulations, the protonation state of the NS2B/NS3 protease was adjusted to physiological pH using the APBS-PDB2PQR software suite (https://server.poissonboltzmann.org/pdb2pqr (accessed on February 27, 2024)).[43] The protonation states of catalytic residues were manually adjusted to align with experimental observations.[24,44] Specifically, catalytic triad residues His37 was protonated on both δ and ε nitrogens, the carboxylic group of Asp61 was deprotonated, and the hydroxyl moiety of Ser121 was deprotonated. These systems are designated as NS2B/NS3 and NS3. The deprotonated serine residue was reparametrized following the guidelines outlined in AMBER's tutorial (https://ambermd.org/tutorials/basic/tutorial5/ (accessed on December 21, 2023)). Trajectories were processed and analyzed using the CPPTRAJ module from Amber Tools.[45]

MD simulations were conducted on the protease with neutral His37 and Ser121, and deprotonated Asp61 residues to comprehend the structural changes in the active site resulting from different protona-

tion states of catalytic residues. This system is denoted as NS2B/NS3 (His37^0/Asp61$^-$/Ser121^0). All other simulation protocols and analyses mirrored those employed for the main NS2B/NS3 protease.

Cluster Analysis: The *k*-means cluster analysis was executed employing pytraj and the CPPTRAJ module for MD trajectory to ascertain the number of NS2B/NS3 complex conformations and their respective populations. The NS2B/NS3 protease structure underwent clustering into four groups, categorized according to the RMSD of residues within the active pocket, namely His37, Arg40, Asp61, Lys118, Ser121, and Asn138. The optimal number of clusters was determined via metrics including DBI, pSF, and SSR/SST.[46] A maximum of 1000 iterations was set, with a randomized initial set of points and a sieving set equal to 10. Representative structures for conformations were identified based on frames closest to the cluster centroids.

Molecular Docking: For 9226 molecules from DrugBank database, ensemble docking was conducted. Three-dimensional structures were extracted from an SDF file downloaded from the DrugBank database[47] and converted to PDBQT format. Similarly, the NS2B/NS3 complexes were prepared in PDBQT format using the Meeko tool developed by the Forli lab at the Center for Computational Structural Biology (CCSB) (https://github.com/forlilab/Meeko (accessed on January 10, 2024)). The center of the cubic grid box, with an edge of 20 Å, was positioned at the CE atom type of the His37 residue. To ensure thorough conformational sampling, the exhaustiveness was set to 100, and all docking poses within 4 kcal mol^{-1} were retained. The final docking score was computed as a weighted binding score across all four conformations, considering the proportion of time the NS2B/NS3 complex spent in each conformation, using formula

$$K_w = \sum_{n=1}^{n} K_i \times p_i \tag{1}$$

K_w represents the ligand's overall weighted non-covalent binding constant, where K_i denotes the ligand's non-covalent binding constant for a specific protein conformation i. The term p_i signifies the proportion of time

**ADVANCED
SCIENCE NEWS**

www.advancedsciencenews.com

**ADVANCED
THEORY AND
SIMULATIONS**

www.advtheorysimul.com

the protein spends in that particular conformation, with *n* indicating the total number of different conformations (in this instance, 4).

Molecular Dynamics Simulation of NS2B/NS3:Drug Complexes: The starting configurations for molecular dynamics simulations of the NS2B/NS3 protein complexed with ligands bound to the active site were obtained from docking experiments. Due to limited computational resources, we perform MD simulations for 6 selected molecules bound for the most populated conformation (**A**). The protein was parameterized using the AMBER ff19SB force field, while ligands were parameterized with the Generalized Amber Force Field (GAFF).[48] The complex was then solvated in a truncated octahedral box with TIP3P water molecules,[49] with a 12 Å buffer region, and neutralized with sodium ions. Sodium (Na^+) and chloride (Cl^-) ions were introduced to achieve a neutral environment with a salt concentration of 0.15 M.[50] The minimization, equilibration, and production protocol followed the same procedure as described for the NS2B/NS3 case. All simulations were performed in triplicate, ensuring robust sampling across independent trajectories.

Free Energy of Binding Calculations: Equally spaced snapshots of each complex were extracted from the MD trajectories at regular intervals of 10 ps. The MM/GBSA method precisely calculates the binding free energy of a ligand–protein complex by comparing the free energy of the complex with the free energies of its individual components (receptor and ligand). This estimation accounts for both entropic and enthalpy terms, and is implemented within the single-trajectory approach in the MMPSBA.py script.[28,51]

$$\Delta G_{bind} = \Delta H - T\Delta S \approx \Delta E_{MM} + \Delta G_{sol} - T\Delta S \qquad (2)$$

$$\Delta E_{MM} = \Delta E_{internal} + \Delta E_{electrostatic} + \Delta E_{vdW} \qquad (3)$$

$$\Delta G_{sol} = \Delta G_{GB} + \Delta G_{SA} \qquad (4)$$

The total binding free energy (ΔG_{bind}) is determined by summing the gas-phase interaction energy between the ligand and protein (ΔE_{MM}), the solvation energy during the transition from gas-phase to solvated state (ΔG_{solv}), and the change of entropy introduced by ligand binding ($-T\Delta S$). $\Delta E_{internal}$ represents the internal energy resulting from bond, angle, and dihedral terms in the MM force field. $\Delta E_{electrostatic}$ and ΔE_{vdW} denote the electrostatic energy and the van der Waals contribution from MM force field, respectively. ΔG_{SA} signifies the nonpolar (nonelectrostatic) component of the solvation free energy determined by an empirical model, while ΔG_{GB} denotes the electrostatic contribution to the solvation free energy. The presented ΔG_{bind} values represent the mean ± standard deviation across all segments. Furthermore, the MM/GBSA free energies of binding were decomposed to assess the per-residue contributions, enabling the identification of key interactions among the residues.

Supporting Information

Supporting Information is available from the Wiley Online Library or from the author.

Acknowledgements

Conflict of Interest

The authors declare no conflict of interest.

Declaration of Generative AI and AI-Assisted Technologies in the Writing Process During the preparation of this work the authors used ChatGPT 3.5 in order to improve readability and language. Image Creator from Microsoft Designer was utilized to create a portion of the graphical abstract. After using this service, the authors reviewed and edited the content as needed and take full responsibility for the content of the publication.

Author Contributions

Conceptualization, J.N. and S.K.; methodology, J.N., S.K. and R.S.; formal analysis, J.N. and S.K.; investigation, J.N. and S.K.; resources, J.N; writing—original draft preparation, J.N. and S.K.; writing—review and editing, J.N., S.K. and R.S.; visualization, J.N; project administration, J.N.; funding acquisition, J.N. All authors have read and agreed to the published version of the manuscript.

Data Availability Statement

The data that support the findings of this study are openly available in the Amber trajectories of NS2B/NS3, NS3, NS2B/NS3:ligand clusters are openly available in FULIR DATA repository at https://data.fulir.irb.hr/islandora/object/irb:705 (accessed on 15 March 2025).

Keywords

[1] A. M. Zaki, *Trans. R. Soc. Tropical Med. Hygiene* **1997**, *91*, 179.
[2] R. N. Charrel, A. M. Zaki, M. Fakeeh, A. I. Yousef, R. de Chesse, H. Attoui, X. de Lamballerie, *Emerg. Infect. Dis.* **2005**, *11*, 683.
[3] (Eds.: A. M. King, M. J. Adams, E. B. Carstens, E. J. Lefkowitz), *Family - Flaviviridae*, Elsevier, Cham **2012**, pp. 1003–1020.
[4] T. Hoffman, M. Lindeborg, C. Barboutis, K. Erciyas-Yavuz, M. Evander, T. Fransson, J. Figuerola, T. G. Jaenson, Y. Kiat, P.-E. Lindgren, Åke Lundkvist, N. Mohamed, S. Moutailler, F. Nyström, B. Olsen, E. Salaneck, *Emerg. Infect. Dis.* **2018**, *24*, 879.
[5] M. Mahdi, B. R. Erickson, J. A. Comer, S. T. Nichol, P. E. Rollin, M. A. AlMazroa, Z. A. Memish, *Emerg. Infect. Dis.* **2011**, *17*, 945.
[6] M. Musso, V. Galati, M. Stella, A. Capone, *J. Clin. Virol.* **2015**, *66*, 12.
[7] T. A. Madani, E. I. Azhar, E.-T. M. Abuelzein, M. Kao, H. M. Al-Bar, H. Abu-Araki, M. Niedrig, T. G. Ksiazek, *J. Infect.* **2011**, *62*, 67.
[8] J. A. Al-Tawfiq, Z. A. Memish, *Microbes Infect.* **2017**, *19*, 305.
[9] K. A. Dodd, B. H. Bird, M. L. Khristova, C. G. Albariño, S. A. Carroll, J. A. Comer, B. R. Erickson, P. E. Rollin, S. T. Nichol, *PLoS Neglect. Tropical Dis.* **2011**, *5*, e1352.
[10] P. Simmonds, P. Becher, J. Bukh, E. A. Gould, G. Meyers, T. Monath, S. Muerhoff, A. Pletnev, R. Rico-Hesse, D. B. Smith, J. T. Stapleton, *J. Gen. Virol.* **2017**, *98*, 2.
[11] A. Fernández-Sanlés, P. Ríos-Marco, C. Romero-López, A. Berzal-Herranz, *Front. Microbiol.* **2017**, *08*.
[12] W. Ng, R. Soto-Acosta, S. Bradrick, M. Garcia-Blanco, E. Ooi, *Viruses* **2017**, *9*, 137.
[13] J. Y. Leung, G. P. Pijlman, N. Kondratieva, J. Hyde, J. M. Mackenzie, A. A. Khromykh, *J. Virol.* **2008**, *82*, 4731.
[14] Z. Li, J. Zhang, H. Li, *Flavivirus NS2B/NS3 Protease: Structure, Function, and Inhibition*, Elsevier, **2017**, pp. 163–188.

ADVANCED
SCIENCE NEWS

www.advancedsciencenews.com

ADVANCED
THEORY AND
SIMULATIONS

www.advtheorysimul.com

[15] T. A. Madani, E.-T. M. E. Abuelzein, *Arch. Virol.* **2021**, *166*, 2357.

[16] B. Bhatia, H. Feldmann, A. Marzi, *Microorganisms* **2020**, *8*, 1406.

[17] Z. A. Memish, S. F. Fagbo, A. M. Assiri, P. Rollin, A. M. Zaki, R. Charrel, C. Mores, A. MacNeil, *PLoS Neglect. Tropical Dis.* **2012**, *6*, e1604.

[18] A. A. Abdulhaq, A. A. Hershan, K. Karunamoorthi, H. M. Al-Mekhlafi, *Saudi J. Biol. Sci.* **2022**, *29*, 1900.

[19] D. Luo, S. G. Vasudevan, J. Lescar, *Antiviral Res.* **2015**, *118*, 148.

[20] M. Bessaud, G. Grard, C. N. Peyrefitte, B. Pastorino, D. Rolland, R. N. Charrel, X. de Lamballerie, H. J. Tolou, *Virus Res.* **2005**, *107*, 57.

[21] S. Kandagalla, J. Novak, S. B. Shekarappa, M. A. Grishina, V. A. Potemkin, B. Kumbar, *J. Biomol. Struct. Dyn.* **2022**, *40*, 13547.

[22] S. Kandagalla, B. Kumbar, J. Novak, *Int. J. Mol. Sci.* **2023**, *24*, 10907.

[23] W. Y. Wahlgren, G. Pál, J. Kardos, P. Porrogi, B. Szenthe, A. Patthy, L. Gráf, G. Katona, *J. Biol. Chem.* **2011**, *286*, 3587.

[24] J. Zephyr, N. K. Yilmaz, C. A. Schiffer, *Viral proteases: Structure, mechanism and inhibition*, **2021**, pp. 301–333.

[25] N. Anede, M. Ouassaf, K. R. R. Rengasamy, S. U. Khan, B. Y. Alhatlani, *Mol. Biotechnol.* **2024**.

[26] H. N. Altayb, H. A. Alatawi, *Pharmaceuticals* **2024**, *17*, 1067.

[27] A. Nasir, A. Samad, A. Ajmal, P. Li, M. Islam, S. Ullah, M. Shah, Q. Bai, *Int. J. Biol. Macromol.* **2024**, *272*, 132855.

[28] S. Genheden, U. Ryde, *Expert Opin. Drug Discov.* **2015**, *10*, 449.

[29] M. U. Mirza, I. Alanko, M. Vanmeert, K. M. Muzzarelli, O. M. Salo-Ahen, I. Abdullah, I. A. Kovari, S. Claes, S. De Jonghe, D. Schols, R. F. Schinazi, L. C. Kovari, J. F. Trant, S. Ahmad, M. Froeyen, *Eur. J. Pharm. Sci.* **2022**, *175*, 106220.

[30] H. M. Rehman, M. Sajjad, M. A. Ali, R. Gul, M. Irfan, M. Naveed, M. A. Bhinder, M. U. Ghani, N. Hussain, A. S. A. Said, A. H. I. Al Haddad, M. Saleem, *Vaccines* **2023**, *11*, 131.

[31] O. Cruz-Arreola, A. Orduña-Diaz, F. Domínguez, J. Reyes-Leyva, V. Vallejo-Ruiz, L. Domínguez-Ramírez, G. Santos-López, *PeerJ* **2022**, *10*, e13650.

[32] S. Clum, K. E. Ebner, R. Padmanabhan, *J. Biol. Chem.* **1997**, *272*, 30715.

[33] P. Erbel, N. Schiering, A. D'Arcy, M. Renatus, M. Kroemer, S. P. Lim, Z. Yin, T. H. Keller, S. G. Vasudevan, U. Hommel, *Nat. Struct. Mol. Biol.* **2006**, *13*, 372.

[34] C. G. Noble, P.-Y. Shi, *Antiviral Res.* **2012**, *96*, 115.

[35] G. Gupta, L. Lim, J. Song, *PLOS One* **2015**, *10*, e0134823.

[36] S. P. Lim, Q.-Y. Wang, C. G. Noble, Y.-L. Chen, H. Dong, B. Zou, F. Yokokawa, S. Nilar, P. Smith, D. Beer, J. Lescar, P.-Y. Shi, *Antiviral Res.* **2013**, *100*, 500.

[37] P. Tfelt-Hansen, P. R. Saxena, C. Dahlöf, J. Pascual, M. Láinez, P. Henry, H. Diener, J. Schoenen, M. D. Ferrari, P. J. Goadsby, *Brain J. Neurol.* **2000**, *123 (Pt 1)*, 9.

[38] D. M. Paton, *Drugs Today* **2016**, *52*, 485.

[39] M. Leivers, J. F. Miller, S. A. Chan, R. Lauchli, S. Liehr, W. Mo, T. Ton, E. M. Turner, M. Youngman, J. G. Falls, S. Long, A. Mathis, J. Walker, *J. Med. Chem.* **2014**, *57*, 1964.

[40] T. H. Evering, M. Markowitz, *Drugs Today* **2007**, *43*, 865.

[41] R. N. Charrel, A. M. Zaki, H. Attoui, M. Fakeeh, F. Billoir, A. I. Yousef, R. de Chesse, P. D. Micco, E. A. Gould, X. de Lamballerie, *Biochem. Biophys. Res. Commun.* **2001**, *287*, 455.

[42] D. A. Case, H. M. Aktulga, K. Belfon, D. S. Cerutti, G. A. Cisneros, V. W. D. Cruzeiro, N. Forouzesh, T. J. Giese, A. W. Götz, H. Gohlke, S. Izadi, K. Kasavajhala, M. C. Kaymak, E. King, T. Kurtzman, T.-S. Lee, P. Li, J. Liu, T. Luchko, R. Luo, M. Manathunga, M. R. Machado, H. M. Nguyen, K. A. O'Hearn, A. V. Onufriev, F. Pan, S. Pantano, R. Qi, A. Rahnamoun, A. Risheh, et al., *J. Chem. Inf. Model.* **2023**, *63*, 6183.

[43] E. Jurrus, D. Engel, K. Star, K. Monson, J. Brandi, L. E. Felberg, D. H. Brookes, L. Wilson, J. Chen, K. Liles, M. Chun, P. Li, D. W. Gohara, T. Dolinsky, R. Konecny, D. R. Koes, J. E. Nielsen, T. Head-Gordon, W. Geng, R. Krasny, G. Wei, M. J. Holst, J. A. McCammon, N. A. Baker, *Protein Sci.* **2018**, *27*, 112.

[44] F. Hofer, J. Kraml, U. Kahler, A. S. Kamenik, K. R. Liedl, *J. Chem. Inf. Model.* **2020**, *60*, 3030.

[45] D. Case, H. Aktulga, K. Belfon, I. Ben-Shalom, J. Berryman, S. Brozell, D. Cerutti, T. I. Cheatham, G. Cisneros, V. Cruzeiro, T. Darden, N. Forouzesh, G. Giambaşu, T. Giese, M. Gilson, H. Gohlke, A. Goetz, J. Harris, S. Izadi, S. Izmailov, K. Kasavajhala, M. Kaymak, E. King, A. Kovalenko, T. Kurtzman, T. Lee, P. Li, C. Lin, J. Liu, T. Luchko, et al., Amber 2023, **2023**.

[46] J. Shao, S. W. Tanner, N. Thompson, T. E. Cheatham, *J. Chem. Theory Comput.* **2007**, *3*, 2312.

[47] C. Knox, M. Wilson, C. Klinger, M. Franklin, E. Oler, A. Wilson, A. Pon, J. Cox, N. E. Chin, S. Strawbridge, M. Garcia-Patino, R. Kruger, A. Sivakumaran, S. Sanford, R. Doshi, N. Khetarpal, O. Fatokun, D. Doucet, A. Zubkowski, D. Rayat, H. Jackson, K. Harford, A. Anjum, M. Zakir, F. Wang, S. Tian, B. Lee, J. Liigand, H. Peters, R. Q. Wang, et al., *Nucleic Acids Res.* **2024**, *52*, D1265.

[48] J. Wang, R. M. Wolf, J. W. Caldwell, P. A. Kollman, D. A. Case, *J. Comput. Chem.* **2004**, *25*, 1157.

[49] W. L. Jorgensen, J. Chandrasekhar, J. D. Madura, R. W. Impey, M. L. Klein, *J. Chem. Phys.* **1983**, *79*, 926.

[50] M. R. Machado, S. Pantano, *J. Chem. Theory Comput.* **2020**, *16*, 1367.

[51] G. Rastelli, A. D. Rio, G. Degliesposti, M. Sgobba, *J. Comput. Chem.* **2010**, *31*, 797.